Inorg. Chem. **2003**, *42*, 6366–6378

Structure-Dependent Photophysical Properties of Singlet and Triplet Metal-to-Ligand Charge Transfer States in Copper(I) Bis(diimine) Compounds

Zainul Abedin Siddique, Yuichi Yamamoto, Takeshi Ohno, and Koichi Nozaki*

Department of Chemistry, Graduate School of Science, Osaka University, 1-16 Machikaneyama, Toyonaka, Osaka 560-0043, Japan

Received April 19, 2003

The photophysical properties of singlet and triplet metal-to-ligand charge transfer (MLCT) states of $[Cu(I)(diimine)_2]^+$, where diimine is 2,9-dimethyl-1,10-phenanthroline (dmphen), 2,9-dibutyl-1,10-phenanthroline (dbphen), or 6,6′-dimethyl-2,2′-bipyridine (dmbpy), were studied. On 400 nm laser excitation of $[Cu(dmphen)_2]^+$ in CH_2Cl_2 solution, prompt ^{1}MLCT fluorescence with a quantum yield of $(2.8 \pm 0.8) \times 10^{-5}$ was observed using a picosecond time-correlated single photon counting technique. The quantum yield was dependent on the excitation wavelength, suggesting that relaxation of the Franck–Condon state to the lowest ^{1}MLCT competes with rapid intersystem crossing (ISC). The fluorescence lifetime of the copper(I) compound was 13–16 ps, unexpectedly long despite a large spin–orbit coupling constant of 3d electrons in copper (829 cm^{-1}). Quantum chemical calculations using a density functional theory revealed that the structure of the lowest ^{1}MLCT in $[Cu(dmphen)_2]^+$ (1^1B_1) was flattened due to the Jahn–Teller effect in $3d^9$ electronic configuration, and the dihedral angle between the two phenanthroline planes (dha) was about 75° with the dha around 90° in the ground state. Intramolecular reorganization energy for the radiative transition of 1^1B_1 was calculated as 2.1×10^3 cm^{-1}, which is responsible for the large Stokes shift of the fluorescence observed (5.4×10^3 cm^{-1}). To understand the sluggishness of the intersystem crossing (ISC) of ^{1}MLCT of the copper(I) compounds, the strength of the spin–orbit interaction between the lowest ^{1}MLCT (1^1B_1) and all ^{3}MLCT states was calculated. The ISC channels induced by strong spin–orbit interactions (ca. 300 cm^{-1}) between the metal-centered HOMO and HOMO − 1 were shown to be energetically unfavorable in the copper(I) compounds because the flattening distortion caused large splitting (6.9×10^3 cm^{-1}) between these orbitals. The possible ISC is therefore induced by weak spin–orbit interactions (ca. 30 cm^{-1}) between ligand-centered molecular orbitals. Further quantum mechanical study on the spin–orbit interaction between the lowest ^{3}MLCT (1^3A) and all ^{1}MLCT states indicated that the phosphorescence borrows intensity from 2^1B_1. The radiative rate of the phosphorescence was also structure-sensitive. The flattening distortion reduced the transition dipole moment of $2^1B_1 \rightarrow$ the ground state, and decreased the extent of mixing between 1^3A and 2^1B_1, thereby considerably reducing the phosphorescence radiative rate at the MLCT geometry compared to that at the ground state geometry. The theoretical calculation satisfactorily reproduced the radiative rate of ca. 10^3 s^{-1} and accounted for the structure-sensitive phosphorescence intensities of copper(I) bis(diimine) compounds recently demonstrated by Felder et al. (Felder, D.; Nierengarten, J. F.; Barigelletti, F.; Ventura, B.; Armaroli, N. *J. Am. Chem. Soc*. **2001**, *123*, 6291).

Introduction

Photoluminescent ruthenium(II) bis(diimine) compounds have been extensively studied for light harvesting devices in dye-sensitized solar cells.[1−3] Transient absorption measurements have shown that the electron injection from a metal-to-ligand charge transfer state (MLCT) of ruthenium dye $[Ru(bpy\text{-}4,4'\text{-}(COOH)_2)_2(NCS)_2]$ to titanium dioxide (TiO_2) film was at least biphasic with ca. 50% in <150 fs and 50% in 1.2 ± 0.2 ps.[4] From an economical viewpoint,

* To whom correspondence should be addressed. E-mail: nozaki@ch.wani.osaka-u.ac.jp.

(1) Felder, D.; Nierengarten, J. F.; Barigelletti, F.; Ventura, B.; Armaroli, N. *J. Am. Chem. Soc*. **2001**, *123*, 6291.
(2) Juris, A.; Balzani, V.; Barigelletti, F.; Campagna, S.; Belser, P.; Zelewsky, A. V. *Coord. Chem. Rev.* **1988**, *84*, 85.

10.1021/ic034412v CCC: $25.00
Published on Web 09/04/2003

first-transition metal compounds have been studied as candidates for sensitizers. An ultrafast electron injection was reported to occur from MLCT of $[Fe(bpy\text{-}4,4'\text{-}(COOH)_2)_2](CN)_2$.[5] Various copper(I) bis(diimine) compounds have also been studied as copper(I) bis(diimine) compounds absorb over a wide region of solar light and exhibit longer-lived MLCT emission in the nanosecond region. Thus, copper(I) compound studies have attracted much interest recently in the development of solar energy conversion processes.[6]

Much of the pioneering work with copper(I) compounds has been accomplished by McMillin and co-workers.[7−18] Studies on the photophysical, structural, and electrochemical properties of Cu(I) compounds have also been investigated by other groups.[19−22] $[Cu(dmphen)_2]^+$, where dmphen is 2,9-dimethyl phenanthroline, is luminescent in dichloromethane (steady state emission quantum yield (Φ) = ca. 2×10^{-4})[8,9] upon excitation of the MLCT band at room temperature, whereas $[Cu(I)(1,10\text{-phenanthroline})_2]^+$ shows no emission in the same experimental condition. Substituents at 2,9-positions of 1,10-phenanthroline are primarily responsible for the emission as they can sterically prevent large structural distortion (e.g., flattening or rocking distortion) due to the Jahn−Teller effect in the MLCT.[10] The theoretical ground of the structure change on the MLCT formation of copper(I) compounds has been reported by Sakaki et al.[23] Spectroscopic study and DV-Xα molecular orbital calculation showed that the lowest MLCT transition energy is red-shifted and the emission lifetime is reduced by decreasing the dihedral angle (dha) between two ligands in $[Cu(dmphen)_2]X$ ($X = BF_4^-$, ClO_4^-, NO_3^-, and Cl^-).[20] The distortion of the pseudotetrahedral structure in MLCT states of $[Cu(dmphen)_2]^+$ was directly measured with nanosecond X-ray pulses.[24] Structure-sensitive phosphorescence intensity was very recently demonstrated by Felder et al., and as such, long alkyl chains in the 2,9-positions of phenanthroline in copper(I) bis(diimine) compounds are able to prevent significant excited state distortions in the rigid matrix.[1]

The origin of the emission in $[Cu(diimine)_2]^+$ is still ambiguous. The temperature dependence of the emission intensity indicated that the emission originates from the thermally equilibrated upper state at an ambient temperature.[11] The higher state was assigned as ^{1}MLCT on the basis of its high radiative rate constant of $>10^7$ s^{-1}.[11] Contrary to this assignment, Parker et al. have assessed the emission as originating entirely from an ^{3}MLCT on the basis of its large Stokes shift ($\sim$5600 cm^{-1}).[22] A rapidly decaying transient emission ($\leq$10 ns) was observed when $[Cu(dmphen)_2]^+$ in CH_2Cl_2 was excited with a nanosecond pulse laser at around −30 °C.[11] In the time-resolved emission spectra of $[Cu(PPh_3)_2(phen)]^+$ at low temperatures (77−90 K), a weak and short-lived (<1 ns) component was observed and assessed as fluorescence from the ^{1}MLCT.[12] However, no MLCT fluorescence has been observed in most transition metal compounds so far because fairly large spin−orbit coupling of d electrons induces very rapid intersystem crossing. Ultrafast pump−probe measurements have demonstrated that the formation of ^{3}MLCT in $[Ru(bpy)_3]^{2+}$ was completed within 100 fs.[25] Very recently, the lifetime of prompt fluorescence from ^{1}MLCT of the ruthenium compound was determined to be only 40 ± 15 fs by means of an up-conversion technique, and the quantum yield was estimated to be less than 10^{-6}.[26] The spin−orbit coupling constant (829 cm^{-1}) of 3d electrons in copper(I) is almost comparable to that of 4d electrons in ruthenium(II) (990 cm^{-1}).[27,28] Thus, a question arises regarding the unexpected strong intensity of the prompt fluorescence from ^{1}MLCT in these copper(I) compounds.

In this study, short-lived emissions from copper(I) bis(diimine) compounds were examined using a time-correlated single photon counting (TCSPC) technique with picosecond time resolution. The ^{1}MLCT lifetime of copper(I) bis(diimine) compounds was 13−16 ps, ca. 400 times longer than that of $[Ru(bpy)_3]^{2+}$.[26] We rationalized the unexpectedly long lifetime of ^{1}MLCT on the basis of quantum chemical calculations using density functional theory (DFT). Analysis of the spin−orbit interaction between the lowest ^{1}MLCT and all ^{3}MLCT states revealed that the flattening distortion in MLCT was responsible for the sluggishness of the intersystem crossing in these copper(I) compounds. The origin of

(3) Meyer, T. J. *Acc. Chem. Res*. **1989**, *22*, 163.
(4) Kalyanasundaram, K. *Coord. Chem. Rev*. **1982**, *46*, 159.
(5) Tachibana, Y.; Moser, J. E.; Gratzel, M.; Klug, D. R.; Durrant, J. R. *J. Phys. Chem.* **1996**, *100*, 20056.
(6) Ferrere, S.; Gregg, B. A. *J. Am. Chem. Soc*. **1998**, *120*, 843.
(7) Eggleston, M. K.; McMillin, D. R.; Koenig, K. S.; Pallenberg, A. J. *Inorg. Chem*. **1997**, *36*, 172.
(8) Blaskie, M. W.; McMillin, D. R. *Inorg. Chem*. **1980**, *19*, 3519.
(9) McMillin, D. R.; Kirchhoff, J. R.; Goodwin, K. V. *Coord. Chem. Rev*. **1985**, *64*, 83.
(10) Cunningham, C. T.; Moore, J. J.; Cunningham, K. L. H.; Fanwick, P. E.; McMillin, D. R. *Inorg. Chem*. **2000**, *39*, 3638.
(11) Kirchhoff, J. R.; Gamache, R. E.; Blaskie, M. W.; Paggio, A. D.; Lengel, R. K.; McMillin, D. R. *Inorg. Chem*. **1983**, *22*, 2380.
(12) Buckner, M. T.; Matthews, T. G.; Lytle, F. E.; McMillin, D. R. *J. Am. Chem. Soc*. **1979**, *101*, 5846.
(13) Ichinaga, A. K.; Kirchoff, J. R.; McMillin, D. R.; Dietrich-Buchecker, C. O.; Marnot, P. A.; Sauvage, J. P. *Inorg. Chem*. **1987**, *26*, 4290.
(14) Cunningham, C. T.; Cunningham, K. L. H.; Michalec, J. F.; McMillin, D. R. *Inorg. Chem*. **1999**, *38*, 4388.
(15) Burke, P. J.; McMillin, D. R.; Robinson, W. R. *Inorg. Chem.* **1980**, *19*, 1211.
(16) Palmer, C. E. A.; McMillin, D. R.; Kirmaier, C.; Holten, D. *Inorg. Chem.* **1987**, *26*, 3167.
(17) Everly, R. M.; McMillin, D. R. *Photochem. Photobiol*. **1989**, *6*, 711.
(18) Everly, R. M.; McMillin, D. R. *J. Phys. Chem.* **1991**, *95*, 9071.
(19) Miller, M. T.; Gantzel, P. K.; Karpishin, T. B. *Inorg. Chem*. **1999**, *38*, 3414.
(20) Shinozaki, K.; Kaizu, Y. *Bull. Chem. Soc. Jpn*. **1994**, *67*, 2435.
(21) (a) Scaltrio, D. V.; Thompson, D. W.; O'Callaghan, J. A.; Meyer, G. J. *Coord. Chem. Rev.* **2000**, *208*, 243. (b) Ruthosky, M. R.; Kelly, C. A.; Castellano, F. N.; Meyer, G. J. *Coord. Chem. Rev.* **1998**, *171*, 309.
(22) Parker, W. L.; Crosby, G. A. *J. Phys. Chem*. **1989**, *93*, 5692.
(23) Sakaki, S.; Mizutani, H.; Kase, Y. *Inorg. Chem*. **1992**, *31*, 4375.
(24) Chen, L. X.; Jennings, G.; Liu, T.; Gosztola, D. J.; Hessler, J. P.; Scaltrito, D. V.; Meyer, G. J. *J. Am. Chem. Soc*. **2002**, *124*, 10861.
(25) (a) Damrauer, N. H.; Cerullo, G.; Yeh, A.; Shank, C. V.; McCusker, J. K. *Science* **1997**, *275*, 54. (b) Yeh, A. T.; Shank, C. V.; McCusker, J. K. *Science* **2000**, *289*, 935.
(26) Bhasikuttan, A. C.; Suzuki, M.; Nakashima, S.; Okada, T. *J. Am. Chem. Soc*. **2002**, *124*, 8398.
(27) (a) Griffith, J. S. *The Theory of Transition-Metal ions*; Cambridge University Press: London, 1964; p 113. (b) Khudyakov, I. V.; Serebremnikov, Y. A.; Turro, N. J. *Chem. Rev*. **1993**, *93*, 537. (c) Bendix, J.; Brorson, M.; Schaffer, C. E. *Inorg. Chem*. **1993**, *32*, 2838. (d) Sugar, J.; Musgrove, A. *J. Phys. Chem. Ref. Data* **1990**, *19*, 527.
(28) Murov, S. L.; Carmichael, I.; Hug, G. L. *Handbook of Photochemistry*, 2nd ed.; Marcel Dekker: New York, 1993; p 9.

the phosphorescence in $[Cu(dmphen)_2]^+$ was also studied theoretically.

Experimental Section

(I) Materials. *n*-Butyllithium was purchased from Aldrich Chemical Co. Dichloromethane (CH_2Cl_2), acetonitrile, and toluene used for spectral measurements were a special grade for fluorescence measurements (Nacalai Tesque, Inc.). All other chemicals were of analytical grade and were used as received. Bis(2,9-*n*-butyl)-phenanthroline was synthesized as described in the literature[29] and then purified on a silica gel chromatographic column (1.5 cm × 20 cm) where 1−5% methanol in CH_2Cl_2 was used as the eluant. This ligand was recrystallized several times in pentane. $[Cu(dmphen)_2]PF_6$, $[Cu(dbphen)_2]PF_6$, and $[Cu(dmbpy)_2]PF_6$ were synthesized according to the literature.[29] The compounds, after several recrystallizations, were purified in an activated alumina column (1.5 cm × 20 cm) with 1−10% acetonitrile in CH_2Cl_2 as the eluant. Further purifications were undergone for all these compounds by recrystallization in water. Elemental analyses and ^1H NMR spectra were used to ascertain the purity.

$[Cu(dmphen)_2]PF_6$. Anal. Calcd for $C_{28}H_{24}N_4CuPF_6$: C, 53.81; H, 3.87; N, 8.96. Found: C, 53.81; H, 4.01; N, 8.97

$[Cu(dbphen)_2]PF_6$. Anal. Calcd for $C_{40}H_{48}N_4CuPF_6$: C, 60.56; H, 6.10; N, 7.10. Found: C, 60.63; H, 6.16; N, 7.12

$[Cu(dmbpy)_2]PF_6$. Anal. Calcd for $C_{24}H_{24}N_4CuPF_6$: C, 49.96; H, 4.19; N, 9.71. Found: C, 49.87; H, 4.23; N, 9.71

(II) Instrumentation. Emission spectra (steady state) were recorded using a grating monochromator (Triax 1900) with a CCD image sensor (Hamamatsu S7031). The spectral sensitivity of the spectrofluorometer was corrected using a bromine lamp (Ushio IPD 100V 500WCS). A sample in a 1 cm quartz cell was excited using an argon ion laser (488 nm, 100 mW, INNOVA 300, Coherent Co.). A cryostat (Oxford ND-1740) with a temperature controller (Oxford ITC-502) was used. Picosecond time-resolved emission spectra were measured using two time-correlated single photon counting (TCSPC) systems. To determine the emission lifetime, a sample solution in a 1 mm quartz cell was excited with the second harmonics (400 nm, 700 kHz repetition rate) of a lab-constructed cavity-dumped mode-locked Ti^{3+}-sapphire laser. To measure the emission spectra, the second harmonics (400 nm, 10−50 mW, 80 MHz repetition rate) of a mode-locked Ti^{3+}-sapphire laser (Tsunami Spectra Physics) were used for excitation. The TCSPC data were recorded every 10 nm in the range 550−810 nm. One set of data was scanned within 15−30 min. Emission spectra were constructed by accumulating the 5 sets of data. The instrumental response function (IRF) of the TCSPC system was 35 ps at the full width at half-maximum (fwhm). The details of the TCSPC system are described elsewhere.[30] Depolarized light was used in all cases for the determination of the emission quantum yield.

(III) Determination of Quantum Yield Using TCSPC. Quantum yields of prompt fluorescence (Φ_{prompt}) of the copper(I) compounds were determined from TCSPC data using eq 1:

$$\Phi_{prompt} = \Phi_{ref} \frac{\int\int I(\tilde{\nu},t)\, d\,\tilde{\nu}\, dt}{\int\int I_{ref}(\tilde{\nu},t)\, d\tilde{\nu}\, dt} \cdot \frac{1-10^{-A_{ref}}}{1-10^{-A}} \cdot \frac{n^2}{n_{ref}^2} \qquad (1)$$

where Φ_{ref} is the quantum yield of a reference compound, A is the absorbance at the excitation wavelength, and n is the refractive index of the respective solvent. $I(\tilde{\nu},t)$ is the time profile of the counted photons at each wavenumber ($\tilde{\nu}$) obtained after correction of the spectrum sensitivity of the TCSPC system. For the copper(I) compounds, $I(\tilde{\nu}, t)$ was well fitted to eq 2:

$$I(\tilde{\nu},t) = \mathrm{IRF}(t)*[B_1(\tilde{\nu})\exp(-t/\tau_1) + B_2(\tilde{\nu})\exp(-t/\tau_2)] \qquad (2)$$

where the asterisk (*) is the convolution operator and IRF(t) denotes the instrumental response function; $B_1(\tilde{\nu})$, $B_2(\tilde{\nu})$ are intensities at $t = 0$ for the prompt (τ_1) and delayed lifetime (τ_2) components, respectively. Finally, eq 1 is simplified as

$$\Phi_{prompt} = \Phi_{ref} \frac{\int B_1'(\tilde{\nu})\, d\tilde{\nu}\cdot B_1(\tilde{\nu}_{max})\tau_1}{\int B_{ref}'(\tilde{\nu})\, d\tilde{\nu}\cdot B_{ref}(\tilde{\nu}_{max,ref})\tau_{ref}} \cdot \frac{1-10^{-A_{ref}}}{1-10^{-A}} \cdot \frac{n^2}{n_{ref}^2} \qquad (3)$$

where $B_1'(\tilde{\nu})$ and $B_{ref}'(\tilde{\nu})$ are normalized spectra of the sample and reference, respectively. As the emission spectra of the short-lived species of the copper(I) compounds were not measured in a wavenumber region lower than 12×10^3 cm^{-1}, the spectra in calculating $\int B_1'(\tilde{\nu})\, d\tilde{\nu}$ were assumed to be symmetrical.

In determining the quantum yields using TCSPC, we used 2-aminoanthraquinone (emission quantum yields (Φ_{em}) = 0.012 and lifetime (τ) = 740 ps, air saturated solution) and 8-anilino-1-naphthalene sulfonic acid (Φ_{em} = 0.0028 and τ = 200 ps, air saturated solution) as reference compounds in view of their wider absorption region, moderate quantum yields and lifetimes. These Φ_{em} values were determined using 9,10-diphenylanthracene (Φ_{em} = 0.91, deaerated solution)[28] as a standard compound and were close to the reported values (Φ_{em} = 0.008 for 2-aminoanthraquinone[29] and Φ_{em} = 0.003 for 8-anilino-1-naphthalene sulfonic acid).[30] The dependence of the quantum yield on the excitation wavelength was measured using two methods. Method a: Assuming that the Φ_{em} of 2-aminoanthraquinone is independent of the excitation wavelength, the quantum yields of prompt fluorescence of the copper(I) compounds are determined at the excitation wavelengths of 380, 400, and 430 nm. Method b: The relative quantum yields of the same sample are determined from the ratio of counted photons from the sample and the total number of absorbed photons calculated from the energy of the excitation pulse and absorbance of the sample.

(IV) Computational Chemistry. Density functional calculations were carried out using the Amsterdam Density Functional program package (version 1999).[31−33] An uncontracted triple −ζ Slater-type orbital (STO) basis set with one polarization function was used for the C, N, and H atoms. For Cu, a triple −ζ, 3s, 3p, 3d, and 4s basis with one 4p STO was used. The cores (C, N, 1s; Cu, 1s−2p) were kept frozen. The generalized gradient approximated (GGA) potentials by Becke[34] and Perdew[35] were employed for geometry optimization. The Van Leeuwen-Baerends potentials (LB 94)[36] were used to calculate the excitation energy using the time-dependent density functional theory (TDDFT).[37]

(29) Pallenberg, A. J.; Koenig, K. S.; Barnhart, D. M. *Inorg. Chem*. **1995**, *34*, 2833.
(30) Tsushima, M.; Ikeda, N.; Nozaki, K.; Ohno, T. *J. Phys. Chem. A*. **2000**, *104*, 5176.
(31) Inoue, H.; Hida, M.; Nakashima, N.; Yoshihara, K. *J. Phys. Chem.* **1982**, *86*, 3184.
(32) Robinson, G. W.; Robbins, R. J.; Fleming, G. R.; Morris, J. M.; Knight, A. E. W. *J. Am. Chem. Soc*. **1978**, *100*, 7145.
(33) (a) Baerends, E. J.; Ellis, D. E.; Ros, P. *Chem. Phys*. **1993**, *2*, 42. (b) Boerrigter, P. M.; Velde, G. te.; Baerends, E. J. *Int. J. Quantum Chem.* **1988**, *33*, 87. (c) Velde, G. te.; Baerends, E. J. *J. Comput. Phys*. **1992**, *99*, 84.
(34) Becke, A. D. *Phys. Rev. A* **1988**, *38*, 3098.
(35) Perdew, J. P. *Phys. Rev. B* **1986**, *33*, 8822.
(36) van Leeuwen, R.; Baerends, E. J. *Phys. Rev. A* **1994**, *49* (4), 2421.
(37) Gross, E. K. U.; Dobson, J. F.; Petersilka, M. In *Density Functional Theory*; Nalewajski, R. F., Ed.; Springer: Heidelberg, 1996.

(V) Calculation of Spin−Orbit Integrals. The following assumptions were made to simplify the calculation of spin−orbit integrals between the MLCT states of the copper(I) compounds: (a) The integral was calculated using a one-electron one-center operator

$$H_{SO} = \zeta \sum_{i}^{Nel} l_i \cdot s_i \tag{4}$$

(b) The excited state is represented as a one-electron excitation configuration between two molecular orbitals ($\phi_i \rightarrow \phi_j$). (c) Spin−orbit coupling involving light atoms (C, N, H) is ignored. (d) MO (ϕ) is represented by the linear combination of atomic orbital (LCAO) approximation,

In consideration of these assumptions, the spin−orbit integrals between two excited states are reduced to those between any two 3d atomic orbitals centered on copper(I).

In the D_2 point group, three components of the spin functions of triplet states, $|X\rangle = 1/\sqrt{2}|\beta\beta - \alpha\alpha\rangle$, $|Y\rangle = i/\sqrt{2}|\beta\beta + \alpha\alpha\rangle$, and $|Z\rangle = 1/\sqrt{2}|\alpha\beta + \beta\alpha\rangle$, have B_3, B_2, and B_1 symmetry, respectively.[38] Since H_{SO} is totally symmetric, the spin−orbit integrals have nonzero values only when both spin−orbit functions of singlet and triplet states are at the same symmetry. For example, in the integral between $1^1B_1(21b_2 \rightarrow 22b_3)$ and $1^3A(21b_2 \rightarrow 22b_2)$, the following integral has only a nonzero value.

$$\langle {}^1\Phi_{1B1}|H_{SO}|{}^3\Phi^Z_{1A}\rangle = \frac{1}{2}\zeta\langle \phi_{21b2}{}^{\alpha}\phi_{22b3}{}^{\beta} - \phi_{21b2}{}^{\beta}\phi_{22b3}{}^{\alpha}|l\cdot s|\phi_{21b2}{}^{\alpha}\phi_{22b2}{}^{\beta} + \phi_{21b2}{}^{\beta}\phi_{22b2}{}^{\alpha}\rangle = \frac{1}{2}\zeta[\langle \phi_{22b3}{}^{\beta}|l\cdot s|\phi_{22b2}{}^{\beta}\rangle - \langle \phi_{22b3}{}^{\alpha}|l\cdot s|\phi_{22b2}{}^{\alpha}\rangle] \tag{5}$$

where ${}^1\Phi_{1B1}$ denotes 1^1B_1 state and ${}^3\Phi^Z_{1A}$ is the z-component of spin−orbit function of 1^3A state.

The spin−orbit integrals between MOs are further simplified as a product of the spin−orbit integral between d atomic orbitals and their coefficients.[39] Thus, the spin−orbit integral between ${}^1\Phi_{1B1}$ and ${}^3\Phi^Z_{1A}$ is simply given as eq 6, where C_{yz} ($22b_3$) denotes the coefficient of d_{yz} in $22b_3$ orbital and $C_{xz}(22b_2)$ denotes d_{xz} in the $22b_2$ orbital.

$$\langle {}^1\Phi_{1B1}|H_{SO}|{}^3\Phi^Z_{1A}\rangle = \frac{i}{2}\zeta C_{yz}(11b_3)C_{xz}(22b_2) \tag{6}$$

The spin−orbit coupling constant, ζ, is inversely proportional to the mean cubic radial distribution ($\hat{r}^3$) of the electron and thus depends on the shape of the 3d atomic orbitals. The 3d atomic orbitals used were those optimized as gaseous copper ion for which the spin−orbit coupling constant was determined (829 cm^{-1}).[27,28] Since the difference in shape of the d orbitals between the free copper ion and those of the copper(I) compounds was negligible, the coefficients of these orbitals in MOs were used to evaluate the spin−orbit integrals.

Results

The absorption spectrum of $[Cu(dmphen)_2]^+$ in CH_2Cl_2 showed an intense MLCT (copper(I)-to-ligand charge transfer) band at around 21.9×10^3 cm^{-1} ($\epsilon = 8.4 \times 10^3$ $M^{-1}cm^{-1}$, band II according to the scheme of Ichinaga et al.[13]) and a shoulder at a low wavenumber around 19.5×10^3 cm^{-1} ($\epsilon =$ ca. 1.5×10^3 $M^{-1}cm^{-1}$, band I) (Figure 1a). Similar shapes of MLCT absorption bands were observed in the same spectral region also for $[Cu(dbphen)_2]^+$ or $[Cu(dmbpy)_2]^+$ compounds (Figure 1b,c). The appearance of band I is indicative of flattening distortion of the ground state structure in solution.[14] The peak was observed at around 13.1×10^3 cm^{-1} in the steady state emission spectrum of $[Cu(dmphen)_2]^+$ in CH_2Cl_2 (dotted line in Figure 1a). In temperature-dependent emission spectra (Figure 2), a blue shift and an increase in intensity were observed with an increase in temperature from 173 to 298 K as reported by Kirchoff et al.[11] The emission at 173 K peaked at 11.7×10^3 cm^{-1}, assigned as a transition from ^{3}MLCT. At 298 K, the emission peak energy increased to 13.1×10^3 cm^{-1}, originating from an upper lying emissive state.[11]

When CH_2Cl_2 solutions of these copper(I) compounds were excited with a 400 nm subpicosecond laser pulse, a short-lived emission was detected. Figure 3 demonstrates the time profile of the TCSPC data at 700 nm for $[Cu(dmphen)_2]^+$. The TCSPC data were analyzed using two exponential functions including a convolution of the IRF of the TCSPC system. The lifetime of the short-lived excited state was 13 ps, and the long-lived component was longer than 50 ns. The gated emission spectrum for the short-lived component was obtained by integrating the photons (i.e., relative emission intensity) counted in the time range from −20 to 150 ps at each wavelength (from 550 to 810 nm for $[Cu(dmphen)_2]^+$). The resulting emission spectrum (solid line in Figure 1a) was close to the steady state ones although the peak energy was slightly higher (about 500 cm^{-1}). The peak energy and the lifetime of the short-lived emission are summarized in Table 1. The quantum yield of the short-lived emission was $(2.8 \pm 0.8) \times 10^{-5}$, about one-seventh of that for the steady state emission quantum yield (2.1×10^{-4}) of $[Cu(dmphen)_2]^+$.[11] It has been observed that the short-lived emission quantum yield varied with excitation wavelength. The quantum yields were determined to be 1.7×10^{-5}, 2.0×10^{-5}, and 2.4×10^{-5} at excitations of 380, 400, and 430 nm, respectively (Table 1), provided that the quantum yield of the reference compound (2-amminoanthraquinone) is independent of the excitation wavelength. This wavelength dependency was confirmed by the relative quantum yield determination without using a reference compound (described as method b in the Experimental Section). The radiative rate constants (k_r's) calculated from the decay constants (τ^{-1}'s) and the quantum yields (Φ's) are 2.2×10^6, 1.9×10^6, and 1.4×10^6 s^{-1} for $[Cu(dmphen)_2]^+$, $[Cu(dbphen)_2]^+$, and $[Cu(dmbpy)_2]^+$, respectively (Table 1), assuming that the formation yield of the emissive state is unity. The quantum yield in an acetonitrile solution of $[Cu(dmphen)_2]^+$ was 1.9×10^{-5}, slightly lower than that in CH_2Cl_2.

Quantum Chemical Calculations. To understand the photophysical properties of the copper(I) compounds, a DFT calculation on $[Cu(dmphen)_2]^+$ was performed. First, to check

(38) Transformation matrix of symmetry operations E, $C_2(z)$, $C_2(y)$, and $C_2(x)$ for spin functions, α, β are

$$\begin{pmatrix} 1 & 0 \\ 0 & 1 \end{pmatrix}, \begin{pmatrix} i & 0 \\ 0 & -i \end{pmatrix}, \begin{pmatrix} 0 & 1 \\ -1 & 0 \end{pmatrix}, \text{ and } \begin{pmatrix} 0 & i \\ i & 0 \end{pmatrix}$$

respectively.

(39) A table containing spin−orbit integrals among eight spin−orbitals in D_2 symmetry is shown in Supporting Information.

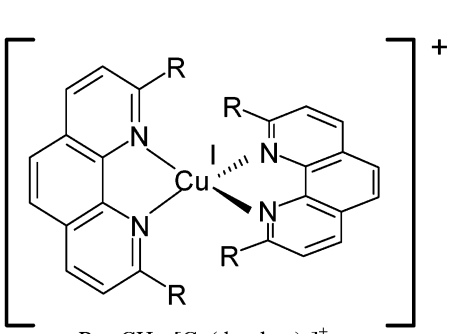

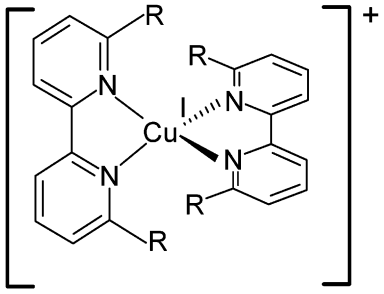

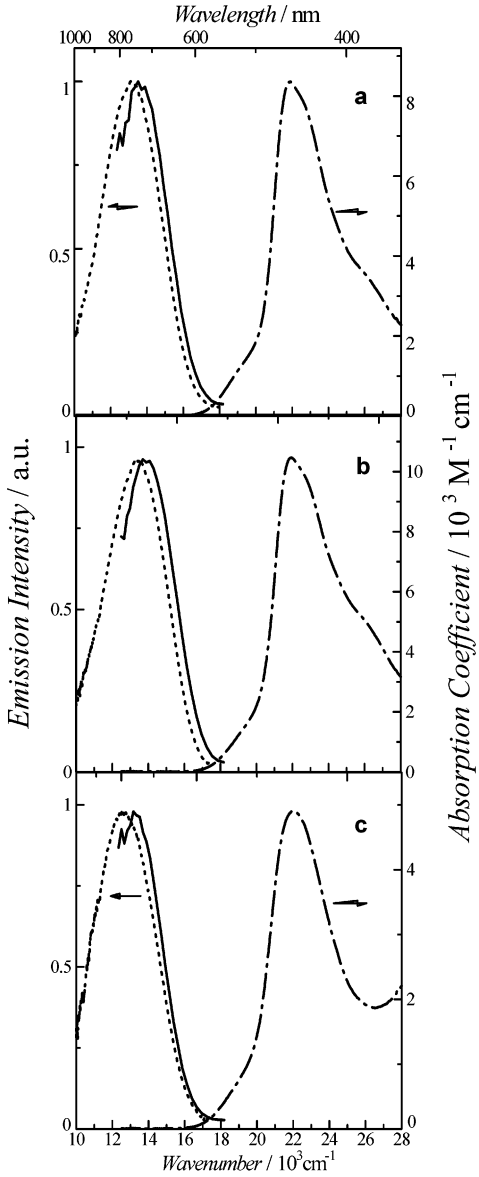

Figure 1. Absorption (— · —), steady state emission (···), and short-lived component in the time-resolved emission (—) spectra in CH_2Cl_2 at 298 K for (a) $[Cu(dmphen)_2]^+$, (b) $[Cu(dbphen)_2]^+$, and (c) $[Cu(dmbpy)_2]^+$ time-gated from −20 to 150 ps, −200 to 50 ps, and −80 to 100 ps, respectively.

Table 1. Peak Energy ($\tilde{\nu}^{max}$), Quantum Yield (Φ), Lifetime (τ), Apparent Radiative Rate (k_r), and Oscillator Strength (f) of Short-Lived Emission of Copper(I) Compounds in CH_2Cl_2 at 298 K

compd	$\tilde{\nu}^{max}/10^3$ cm^{-1}	$\Phi/10^{-5}$ (λ_{ex}/nm)	τ/ps	$k_r/10^6$ s^{-1} [d]	f [e]
$[Cu(dmphen)_2]^+$	13.5	2.8 ± 0.8[b] (400)	13	2.2	0.018
		2.4[c] (430)			
		2.0[c] (400)			
		1.7[c] (380)			
	13.3[a]	1.9[a] (400)	12[a]	1.6[a]	
$[Cu(dbphen)_2]^+$	13.7	3.0 (400)	16	1.9	0.015
$[Cu(dmbpy)_2]^+$	13.2	2.1 (400)	15	1.4	0.012

[a] In acetonitrile at 298 K. [b] Average of 4 data points. [c] Determined in the same condition except for excitation wavelength and assumed that the quantum yield of the reference compound (2-aminoanthraquinone) is independent of the excitation wavelength. [d] Assumed that the quantum yield of the production of fluorescent state from FC state is unity. [e]

$$f = \frac{1.50k_r}{(\tilde{\nu}^{max})^2}$$

the quality of the calculation, the geometry obtained by DFT was compared with the X-ray structure.[40] Most of the bond lengths and angles in the geometry optimized as $[Cu(dmphen)_2]^+$ are in good agreement with the observed ones within 1% error (Figure 4a). One exception is the dihedral angle between the phenanthroline planes (dha). The calculated dha is 90° whereas the observed ones for the crystalline solid $[Cu(NN)_2]X$ complexes (where NN means 2,9-dimethyl-1,10-phenanthroline, 4,4′,6,6′-tetramethyl-2,2′-bipyridine, or 6,6′-dimethyl-2,2′-bipyridine; X is NO_3^-, ClO_4^- or BF_4^-) are 68−81° and depend on the counteranion.[40] The deviation observed in the dha is presumed to be due to packing forces in the crystal.[10]

The excitation energies and the oscillator strengths of ^{1}-MLCT transitions in $[Cu(dmphen)_2]^+$ were calculated using TDDFT as a function of the dha with the other geometry being frozen. The symmetry was set to D_2 in all the calculations. A change in the dha greatly affects the MLCT

(40) Dobson, J. F.; Green, B. F.; Healy, P. C.; Kennard, C. H. L.; Pakawatchai, C.; White, A. H. *Aust. J. Chem.* **1984**, *37*, 649.

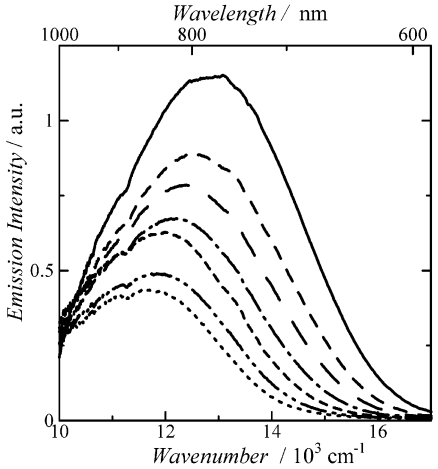

Figure 2. Emission spectra (corrected) of $[Cu(dmphen)_2]^+$ in CH_2Cl_2 at variable temperatures: from top to bottom, 298, 273, 253, 233, 213, 193, and 173 K, respectively.

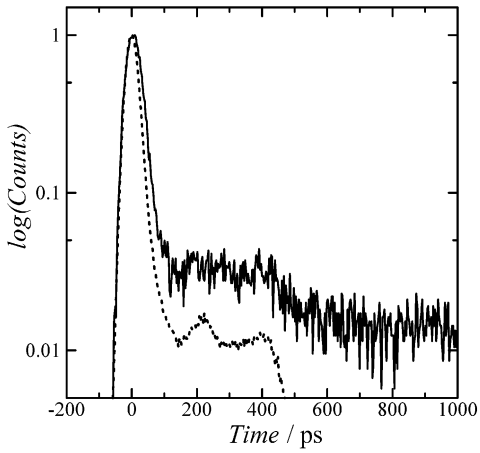

Figure 3. Time profile of TCSPC data at 700 nm for $[Cu(dmphen)_2]^+$ in CH_2Cl_2 when excited with 400 nm; the instrumental response function is shown as a dotted line (···).

transition energies as well as their oscillator strengths. In Table 2, the excitation energy and the oscillator strength for transitions to $^1B_1$ states are summarized. Oscillator strengths of ^{1}MLCT transitions to the other states (^1A, $^1B_2$, and $^1B_3$) are less than 0.007 and are not shown. When the dha was 90°, one ^{1}MLCT transition to $^1B_1$ appeared at 18.5×10^3 cm^{-1} with an oscillator strength of 0.132. Since the lowest $^1B_1$ is denoted by $^1A_2$ in D_{2d} symmetry, the transition to this state is symmetrically forbiden. However, only a slight deviation (ca. 5°) from D_{2d} symmetry allows this transition. By decreasing the dha, namely with flattening distortion from D_{2d} to D_2, the oscillator strength of the transition to the lowest $^1B_1$ state increases, while that of the transition to the higher-lying $^1B_1$ state decreases (Table 2). Excitation energies also depend on the dha. Copper(I) bis(diimine) compounds exhibit two MLCT bands in the visible region, denoted by band I and band II.[13] Band I appears as a shoulder lying on the low-energy side of an intense MLCT band (band II). In the case of $[Cu(dmphen)_2]^+$ in a fluid solution, the peak energy of band I and band II was around 19.5×10^3 and 21.9×10^3 cm^{-1}, respectively. It seems reasonable that the two major transitions around 17×10^3 and 19×10^3 cm^{-1} calculated at the dha of near 90° are assigned to band I and band II,

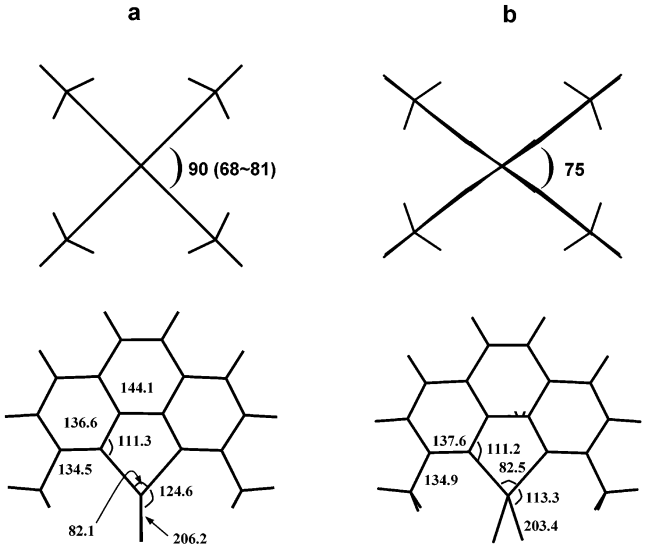

Figure 4. Structures of $[Cu(dmphen)_2]^+$ optimized for the ground state (a) and for the lowest ^{1}MLCT (1^1B_1: $21b_2 \rightarrow 22b_3$) state (b). Some of the bond distanes in picometers and bond angles in degrees are shown together with the observed values for $[Cu(dmphen)_2Br \cdot H_2O]$[40] in parentheses (dha observed for $[Cu(NN)_2]X$, where NN means 2,9-dimethyl-1,10-phenanthroline, 4,4′,6,6′-tetramethyl-2,2′-bipyridine, or 6,6′-dimethyl-2,2′-bipyridine, and X is NO_3^-, ClO_4^-, or BF_4).

respectively, considering the accuracy of TDDFT to be ca. 0.3 eV.[41] The excited states corresponding to band I and band II are mixtures of two electronic configurations described by $21b_2 \rightarrow 22b_3$ and $21b_3 \rightarrow 22b_2$. The molecular orbitals (MOs) of $21b_2$ and $21b_3$ are HOMO and HOMO − 1, respectively, mainly localized on the copper(I) ion.

Figure 5a shows the energy levels of MOs in a singlet ground state (1^1A) at the ground state (GS) geometry (Figure 4a). The MO of $22b_2$ is out of phase, and that of $22b_3$ is an in-phase combination of LUMOs (ϕ) of phenanthrolines. The ϕ orbital is antisymmetric with respect to the C_2 operation of the ligand. When the dha is near 90°, HOMOs ($21b_2$ and $21b_3$) as well as LUMOs ($22b_2$ and $22b_3$) are located at almost the same energy level. As a result, two transitions involving electronic configurations, $21b_2 \rightarrow 22b_3$ and $21b_3 \rightarrow 22b_2$, interact with each other to give two $^1B_1$ states. As the dha decreases, however, the energy of $21b_2$ increases while that of $21b_3$ decreases. Such changes in the orbital energy decrease the excitation energy of $21b_2 \rightarrow 22b_3$ and increase that of $21b_3 \rightarrow 22b_2$. Consequently, when the dha is lower than 80°, two lower-lying $^1B_1$ states are well described as pure electronic transitions, $21b_2 \rightarrow 22b_3$ and $21b_3 \rightarrow 22b_2$, respectively, and the interactions between the two electronic configurations can be ignored.

Figure 6 shows the potential energy curves of the ground and MLCT states versus the dha. All the triplet and singlet states lie in the 2.0−2.4 eV region when dha = 90°. By decreasing the dha, the energy of the MLCT involving $21b_2$ (1^1B_1, 2^1A, 1^1B_3, 1^1B_2 and 1^3A, 1^3B_1, 1^3B_2, 1^3B_3) is lowered and minimized at about dha = 70° whereas the energies of the MLCT involving $21b_3$ (2^1B_1, 3^1A, 2^1B_2, 2^1B_3 and 2^3A, 2^3B_1, 2^3B_2, 2^3B_3) are increased. The results predict that the

(41) Nguyen, K. A.; Day, P. N.; Pachter, R. *J. Chem. Phys.* **1999**, *110*, 9135.

Table 2. Calculated Excitation Energy (E_{ex}) and Oscillator Strength (f) of ^{1}MLCT Transition to Two $^1B_1$ States in $[Cu(dmphen)_2]^+$ (D_2 Symmetry) at Various dha

	dha						
	90°	85°	80°	75°	70°	65°	60°
				Band I			
$E_{ex}/10^3$ cm^{-1}	17.2	16.9	16.4	15.7	15.1	14.4	12.5
f	0	0.021	0.035	0.042	0.043	0.043	0.041
contribution[a]	1: 0.50 2: 0.50	1: 0.87 2: 0.13	1: 0.95	1: >0.98	1: >0.98	1: >0.99	1: >0.99
				Band II			
$E_{ex}/10^3$ cm^{-1}	18.5	18.8	19.3	19.9	20.5	20.9	20.1
f	0.132	0.112	0.094	0.086	0.079	0.071	0.060
contribution[a]	1: 0.50 2: 0.50	1: 0.87 2: 0.13	2: 0.95	2: >0.97	2: >0.98	2: >0.97	2: >0.97

[a] $1 = 21b_2(d_{xz}) \rightarrow 22b_3$ ($\phi + \phi$). $2 = 21b_3(d_{yz}) \rightarrow 22b_2$ ($\phi - \phi$).

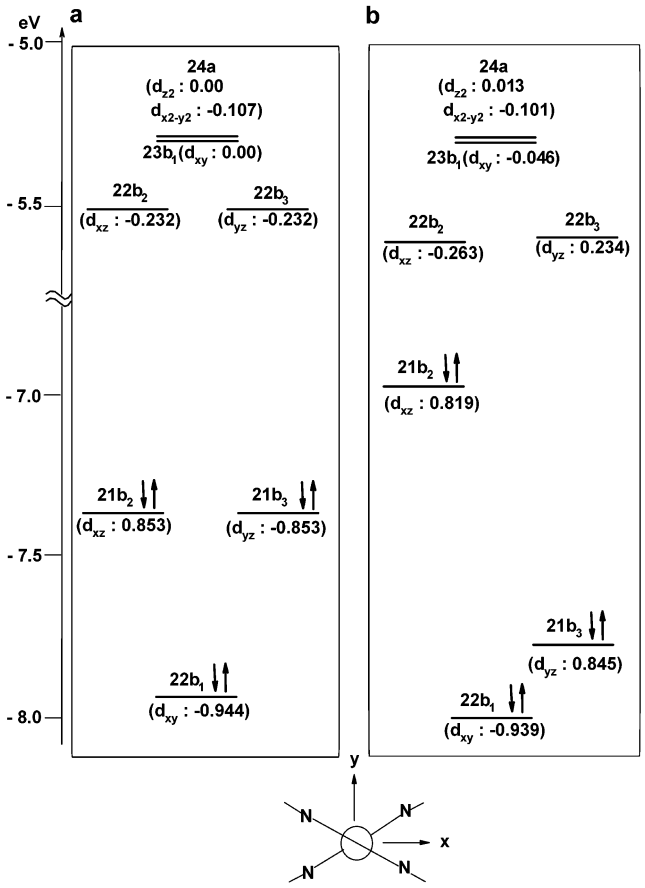

Figure 5. MO energy levels of $[Cu(dmphen)_2]^+$ at the ground state geometry (a) and those at the ^{1}MLCT geometry (b). The numbers in parentheses are coefficients of d orbitals in each MO. The orientation of the molecule in the coordinate system used for calculation is shown at the bottom.

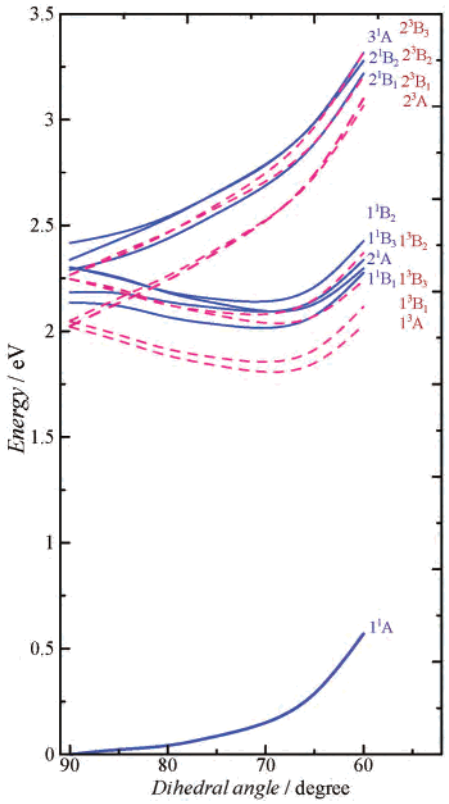

Figure 6. Potential energy curves vs dha for the singlet and the triplet states of $[Cu(dmphen)_2]^+$ by TDDFT calculation are shown by the blue solid line and the red dashed line, respectively.

relaxed structure in the lowest ^{1}MLCT(1^1B_1) will be flattened; i.e., dha is ca. 70°.

Current DFT programs do not have the functionality for geometrical optimization in fluorescent states involving configurational interaction. Fortunately, the relaxed 1^1B_1 in $[Cu(dmphen)_2]^+$ is represented as a simple electronic configuration ($21b_2 \rightarrow 22b_3$) as shown in Table 2. Therefore, the structure at the relaxed 1^1B_1 was obtained after geometry optimization under the restriction of the electronic configuration as $1^1B_1(21b_2 \rightarrow 22b_3)$ within D_2 symmetry.[42] The resulting structure is shown in Figure 4b. The optimized structure is flattened due to the Jahn−Teller effect in the d^9 electronic configuration, and the dihedral angle between two phenanthroline planes (dha) is about 75° whereas the dihedral angle between two N−Cu−N planes is 67.0°. The deviation between these two angles is due to a slight out-of plane distortion of the phenanthroline resulting from the mutual balance between the Jahn−Teller effect and steric hindrance of two methyl groups. The Cu−N bond distance in $[Cu(dmphen)_2]^+$ at the GS geometry is about 206 pm whereas that for the ^{1}MLCT geometry is 203 pm. The N−Cu−N bond angle is 82.5°.

(42) In this calculation, MOs were not fully optimized for the excited state electronic configuration. The resultant ^{1}MLCT geometry is not as reliable as that obtained with wave function based multiconfigurational SCF procedures such as MCSCF or CASPT2.

Table 3. Excitation Energy (E_{ex}) and Oscillator Strength (f) of ^{1}MLCT in $[Cu(dmphen)_2]^+$ at the ^{1}MLCT Geometry

^{1}MLCT	$E_{ex}/10^3$ cm^{-1}, (f)
1^1B_1: $21b_2 \rightarrow 22b_3$	13.3 (4.1×10^{-2})
2^1A: $21b_2 \rightarrow 22b_2$	13.7 (0.0)
1^1B_3: $21b_2 \rightarrow 23b_1$	14.6 (4.2×10^{-3})
1^1B_2: $21b_2 \rightarrow 24a$	14.8 (3.0×10^{-3})
2^1B_1: $21b_3 \rightarrow 22b_2$	19.9 (9.5×10^{-2})
3^1A: $21b_3 \rightarrow 22b_3$	20.9 (0.0)
2^1B_2: $21b_3 \rightarrow 23b_1$	21.6 (5.2×10^{-3})
2^1B_3: $21b_3 \rightarrow 24a$	21.8 (8.4×10^{-3})
3^1B_3: $22b_1 \rightarrow 22b_2$	22.4 (7.6×10^{-4})
3^1B_2: $22b_1 \rightarrow 22b_3$	22.7 (2.9×10^{-4})

Table 4. Excitation Energy (E_{ex}) of ^{3}MLCT in $[Cu(dmphen)_2]^+$ at the ^{1}MLCT Geometry

^{3}MLCT	$E_{ex}/10^3$ cm^{-1}
1^3A: $21b_2 \rightarrow 22b_2$	11.3
1^3B_1: $21b_2 \rightarrow 22b_3$	11.9
1^3B_3: $21b_2 \rightarrow 23b_1$	14.2
1^3B_2: $21b_2 \rightarrow 24a$	14.3
2^3B_1: $21b_3 \rightarrow 22b_2$	18.4
2^3A: $21b_3 \rightarrow 22b_3$	18.5
2^3B_2: $21b_3 \rightarrow 23b_1$	20.7
2^3B_3: $21b_3 \rightarrow 24a$	20.9
3^3B_3: $22b_1 \rightarrow 22b_2$	21.6
3^3B_2: $22b_1 \rightarrow 22b_3$	21.9

A close resemblance was found between the structure at the ^{1}MLCT and that of $[Cu(II)(dmphen)_2]^{2+}$. The calculated bond distance of Cu−N is 204 pm, the N−Cu−N bond angle is 82.7°, and the dha is ca. 75° for the copper(II) compound. These results indicate that the flattening structure at the ^{1}MLCT is almost dominated by a $3d^9$ electronic configuration. In addition, close similarity was also found between the ^{1}MLCT and the ^{3}MLCT geometries. At the latter geometry, the Cu−N bond distance is 204 pm; the N−Cu−N bond angle and dha are 82.4° and about 75°, respectively. The features of the structure changes in the MLCT state, i.e., flattening distortion and shortening of the Cu−N bond distance, are in line with those obtained by the ab initio MO method with the second-order Møller−Plesset perturbation theory for $[Cu(diN)(PH_3)_2]^+$.[23]

The MO energy levels of $[Cu(dmphen)_2]^+$ at the ^{1}MLCT (1^1B_1) geometry are shown in Figure 5b with 3d orbital coefficients. At the GS geometry, where the true symmetry is D_{2d}, two HOMOs ($21b_2$, $21b_3$) and two LUMOs ($22b_3$, $22b_2$) are degenerate (Figure 5a). At the ^{1}MLCT geometry, $21b_2$ is destabilized, and $21b_3$ is stabilized, increasing the energy difference to 6.9×10^3 cm^{-1}. The changes in the orbital energies of HOMOs are due to the change in interaction energy between the 3d orbital and occupied MOs of dmphens. $21b_2$ is the antibonding MO involving $3d_{xz}$, $21b_3$ involves $3d_{yz}$, and the corresponding bonding MOs are located around −11 eV. On changing from the GS to the ^{1}MLCT geometry, the overlap integral between $3d_{xz}$ and the occupied MO increases by 22% (from −0.125 to −0.152) while it decreases to the same extent (22%, from −0.125 to −0.097) for $3d_{yz}$, causing large energy splitting of 6.9×10^3 cm^{-1} between $21b_2$ and $21b_3$. The degenerate LUMOs ($22b_2$ and $22b_3$) also split at the ^{1}MLCT geometry. These MOs are formed as an in-phase and out-of-phase combination of the LUMOs (ϕ) of two phenanthrolines. These MOs are degenerate at the GS geometry because there is no interaction between the ϕ orbitals on the orthogonal phenanthrolines. With flattening distortion, these ϕ orbitals weakly interact through the copper metal, and thus, $22b_2$ and $22b_3$ are split with an energy gap of 520 cm^{-1}, which is double of the strength of the through-copper interaction.

The excitation energy and oscillator strength of all the ^{1}MLCT states of $[Cu(dmphen)_2]^+$ at the MLCT geometry are given in Table 3, and the excitation energies of all the ^{3}MLCT states are listed in Table 4. At the ^{1}MLCT geometry, the transitions to $1^1B_1(21b_2 \rightarrow 22b_3)$ and $2^1B_1(21b_3 \rightarrow 22b_2)$ have the highest oscillator strengths of 0.041 and 0.095, respectively, among all the ^{1}MLCT states. Their excitation energies are 13.3×10^3 and 19.9×10^3 cm^{-1}, respectively. The lowest ^{3}MLCT state at the ^{1}MLCT geometry is 1^3A ($21b_2 \rightarrow 22b_2$) having an excitation energy of 11.3×10^3 cm^{-1}.

Discussion

It is of significant interest to assign the short-lived emission in a picosecond time region (Figure 3). A radiative rate constant (k_r) plays a supportive role in assigning the radiative process to be spin-allowed or spin-forbidden. The radiative rate constants of phosphorescence in the compounds of first series transition metals are estimated to be less than 10^4 s^{-1}.[43] The value of k_r for the short-lived emission in the copper(I) compounds is greater than 10^6 s^{-1} (Table 1), which is significantly greater than that of ^{3}MLCT. Therefore, the short-lived emission is assigned to the prompt fluorescence from ^{1}MLCT. Our assignments in this work support the emission mechanism of the copper(I) compound proposed by Kirchhoff et al.;[11] that is, steady state emission at an ambient temperature is mainly delayed fluorescence. The value of k_r (2.2×10^6 s^{-1}) obtained from direct observation of the prompt fluorescence is, however, about 10 times smaller than that of k_r (2×10^7 s^{-1}) calculated from the temperature-dependent radiative rates of the delayed fluorescence.[11] Furthermore, the observed oscillator strength of $[Cu(dmphen)_2]^+$ in CH_2Cl_2 at 298 K is 0.018 (Table 1), which is smaller than the calculated strength for the transition to 1^1B_1 state (0.04) at the ^{1}MLCT geometry (Table 3). These differences suggest that formation of the fluorescent state from the Franck−Condon (FC) state is not efficient (less than 1).

When the relaxation pathways of the FC state are represented as in Scheme 1, the quantum yield and the radiative rate constant for the prompt fluorescence are expressed as eqs 7 and 8, respectively.

$$\Phi_{prompt} = \frac{k_{41c}}{k_{41c} + k_{42c}} \times \frac{k_{1r}}{k_{1r} + k_{1c} + k_{1n}} = \Phi_{4\rightarrow1} \times \frac{k_{1r}}{k_{1r} + k_{1c} + k_{1n}} = \Phi_{4\rightarrow1} k_{1r} \tau \quad (7)$$

$$k_{1r} = \Phi_{prompt}/\Phi_{4\rightarrow1}\tau \quad (8)$$

There are two possible relaxation pathways from the FC state: one is to the lowest singlet state (k_{41c}), and the other one is to the lowest triplet state (k_{42c}). With the assumption

Scheme 1. Diagram of the Proposed Relaxation Model for Photoexcited $[Cu(dmphen)_2]^{+a}$

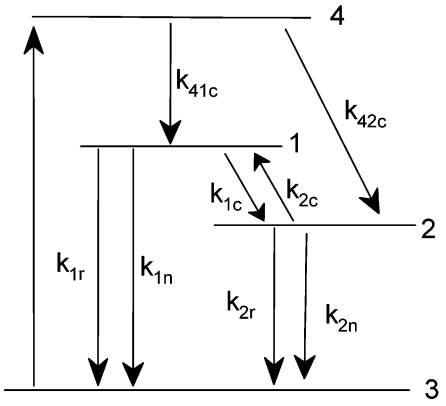

[a] 1, ^{1}MLCT; 2, ^{3}MLCT; 3, GS; 4, FC state.

that $\Phi_{4\rightarrow1}$ equals 1, namely $k_{41c} \gg k_{42c}$, we determined the k_{1r} value to be 2.2×10^6 s^{-1}, that is, about 10 times smaller than 2×10^7 s^{-1} which was determined from the delayed fluorescence. Assuming that k_{1r} in eq 8 is equal to 2×10^7 s^{-1}, one can determine the quantum yield ($\Phi_{4\rightarrow1}$) from the FC state to the lowest singlet state to be 0.1. Such a low $\Phi_{4\rightarrow1}$ value suggests that formation of the lowest ^{1}MLCT from the FC state (k_{41c}) competes with the fast intersystem crossing to ^{3}MLCT (k_{42c}). The quantum yields for the prompt fluorescence of $[Cu(dmphen)_2]^+$ depended on the excitation wavelength, which indicates the presence of competition in the relaxation of the FC states because the ratios of the internal conversion rate (k_{41c}) to the intersystem crossing rate (k_{42c}) is likely to vary with the vibronic state formed on excitation.

The X-ray structures of $[Cu(dmphen)_2]Br\cdot H_2O$[40] and $[Cu(dmbpy)_2]BF_4$[15] disclosed that the dha's between the ligand planes vary in the range 68−81°, smaller than that expected for regular tetrahedral coordination. Each of the Cu−N bond distances (203−205 pm) also shows a small difference for $[Cu(dmphen)_2]Br\cdot H_2O$ which does not match the true D_{2d} symmetry structure. The structure in solution is, however, not the same as that in the crystal, since considerable differences in the absorption spectra have been demonstrated for some copper(I) bis(diimine) compounds[19] and a packing force probably causes flattening distortions in crystals to some extent.[10] Although it is difficult to measure the dha in solution, the structure can be estimated by comparing the observed oscillator strength and the computed strength. Two MLCT absorption bands appear at 19.5×10^3 cm^{-1} (shoulder, band I) and 21.9×10^3 cm^{-1} (band II) having oscillator strengths of 0.016 and 0.135, respectively. The appearance of band I indicates that the dha is not 90° even in solution because band I is symmetrically forbidden at D_{2d} symmetry (dha = 90°) (Table 2). The ratio of the observed oscillator strength of band II to that of band I is ca. 0.12 (= 0.016/0.135), slightly smaller than the ratio of the computed values at dha 85° (0.19) (Table 2). The most probable reason for the slight deviation from 90° is thermal fluctuation because the potential energy curve with respect to the dha is rather shallow around dha = 90° as shown in Figure 6. The calculated energy difference between the structures at 90° and at 85° (177 cm^{-1}) indicates that about 30% of molecules can be thermally populated to the distorted structure of dha = 85° at room temperature. This idea is also supported as the ratio of the intensity of band I to that of band II decreased at 90 K.[13]

The fluorescence from ^{1}MLCT displays a large Stokes shift from band I, about 5.4×10^3 cm^{-1} for $[Cu(dmphen)_2]^+$. As has been noted, the MLCT states of d^{10} metal compounds involve a d^9 electron configuration and then experience appreciable Jahn−Teller effect. Therefore, the copper(I) compounds at the MLCT undergo considerable distortion from the pseudotetrahedral as seen in the structure optimized as ^{1}MLCT (Figure 4b). Such flattening distortion causes a large displacement along the intramolecular coordinate in the ^{1}MLCT against the ground state and thereby produces a large Stokes shift of fluorescence.

The extent of the Stokes shift of the fluorescence for $[Cu(dmphen)_2]^+$ is then examined using DFT. The apparent reorganization energy (λ) for fluorescence is equal to half of the Stokes shift provided that the potential energy curves for both GS and ^{1}MLCT have the same curvature and thus $\lambda = 2.7 \times 10^3$ cm^{-1} in CH_2Cl_2. The reorganization energy (λ) is composed of intramolecular reorganization energy (λ_{in}) and solvent reorganization energy (λ_{out}). The value of λ_{in} for the radiative transition of $^1B_1 \rightarrow$ GS was given as the difference in bonding energy between GS at the ^{1}MLCT geometry (Figure 4b) and GS at the GS geometry (Figure 4a) and was computed to be 2.1×10^3 cm^{-1}. The calculated λ_{in} is close to but 600 cm^{-1} smaller than the observed λ. This small difference may be due to the lowering from the D_2 structure into a distorted trigonal pyramidal accompanied by exciplex formation with the solvent as recently observed using transient X-ray spectroscopy.[24] Thus, most (78%) of the Stokes shift of the fluorescence was reproduced as reorganization energy resulting from the considerable structural difference between ^{1}MLCT and GS.

The temperature dependence of the emission spectrum shows that the intensity is decreased and the peak is red-shifted as the temperature decreases (Figure 2). This temperature-dependent behavior was well explained using a two thermally equilibrated emitting states model, and the energy gap between two states was estimated as 1800 cm^{-1} for $[Cu(dmphen)_2]^+$.[14] The difference in peak energy between the prompt fluorescence and phosphorescence at 173 K (1800 cm^{-1}) is in excellent agreement with this reported value. TDDFT calculation illustrated that the energy difference between the lowest ^{1}MLCT (1^1B_1) and ^{3}MLCT (1^3A) is 2000 cm^{-1}. The agreement confirms that the emission at higher temperatures is delayed fluorescence and both the prompt and the delayed fluorescences occurred as a transition of $1^1B_1 \rightarrow$ GS.

The presence of exciplex or distortion other than flattening in the excited state may reduce the radiative rate constant of 1^1B_1, especially in basic solvents such as acetonitrile. In $[Cu(dmphen)_2]^+$, the apparent radiative rate constant of the

(43) Balzani, V.; Carassitti, V. *Photochemistry of Coordiantion Compounds*; Academic Press: New York, 1970; p 28.

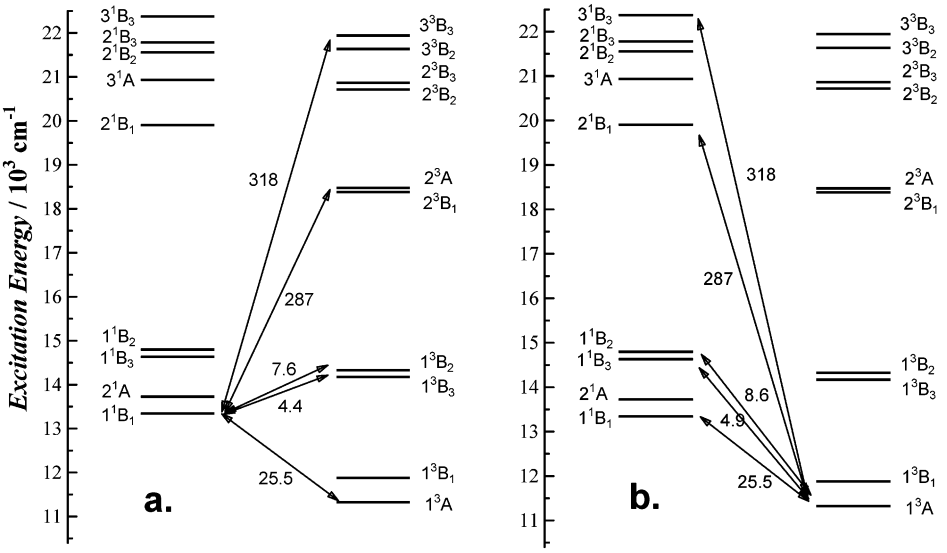

Figure 7. Spin−orbit integrals (cm^{-1}) between 1^1B_1 and triplet states (a) and those between 1^3A and singlet states (b) at the MLCT geometry of $[Cu(dmphen)_2]^+$.

prompt fluorescence was determined as $1.6 \times 10^6\ s^{-1}$ in acetonitrile, slightly smaller than $2.2 \times 10^6\ s^{-1}$ in CH_2Cl_2. Thermodynamic analysis of the nonradiative rates has indicated that the ^{3}MLCT of $[Cu(dmphen)_2]^+$ is in equilibrium with an exciplex of five-coordinated species.[16] Very recent transient X-ray measurements of an MLCT structure of $[Cu(dmphen)_2]^+$ also support the presence of an exciplex with a solvent or counterion. Further theoretical investigations on the photophysical properties of the exciplex are necessary.

The lifetimes of the ^{1}MLCT of copper(I) bis(diimine) compounds are 13−16 ps, ca. 400 times longer than that of Ru(II) MLCT (40 ± 15 fs),[26] although the spin−orbit coupling constant of the 3d electron of copper (829 cm^{-1}) is comparable to that of 4d electrons of Ru (990 cm^{-1}).[27,28] Since the lifetimes of ^{1}MLCT are considered to be dominated by ISC induced by the spin−orbit coupling of the d electrons, understanding the sluggishness of the transition from ^{1}MLCT to ^{3}MLCT in the Cu(I) compounds requires deep insight into the ISC mechanism.

The rate of transition between vibronic states can be expressed as Fermi's golden rule:

$$k(^1\mathrm{MLCT}_m \rightarrow {}^3\mathrm{MLCT}_n) = \frac{2\pi|\langle\psi_{^3\mathrm{MLCT}_n}|V|\psi_{^1\mathrm{MLCT}_m}\rangle|^2}{\hbar}\rho(E_{^3MLCT} = E_{^1\mathrm{MLCT}}) = \frac{2\pi|V_{nm}|^2}{\hbar}\rho(E_{^3MLCT} = E_{^1MLCT}) \quad (9)$$

where $\rho(E_{^3\mathrm{MLCT}} = E_{^1\mathrm{MLCT}})$ is the density of the final vibronic states ($\psi_{^3\mathrm{MLCT}_n}$) having the same energy as the initial states ($\psi_{^1\mathrm{MLCT}_n}$) and V is the perturbation of nuclear kinetic energy T_N and spin−orbit coupling H_{SO}. Siebrand et al. have formulated the matrix elements V_{nm} using the pure spin Born−Oppenheimer functions:[44,45]

$$V_{nm} = V_{nm}^{(1)} + V_{nm}^{(2)} + V_{nm}^{(3)} \quad (10)$$

where

$$V_{nm}^{(1)} = \langle{}^3\Phi_n(q,0)|H_{SO}(0)|{}^1\Phi_m(q,0)\rangle\langle\chi_n|\chi_m\rangle \quad (10a)$$

$$V_{nm}^{(2)} = [(\partial/\partial Q)\langle{}^3\Phi_n(q,Q)|H_{SO}(Q)|{}^1\Phi_m(q,Q)\rangle]_{Q=0}\langle\chi_n|Q|\chi_m\rangle \quad (10b)$$

$$V_{nm}^{(3)} = \left[\sum_i \frac{\langle{}^3\Phi_n|H_{SO}|{}^1\Phi_i\rangle\langle{}^1\Phi_i|T_N|{}^1\Phi_m\rangle}{E_i - E_m} + \sum_j \frac{\langle{}^3\Phi_n|T_N|{}^3\Phi_j\rangle\langle{}^3\Phi_j|H_{SO}|{}^1\Phi_m\rangle}{E_j - E_m}\right] \quad (10c)$$

Here, $\Phi(q,Q)$ and $\chi(Q)$ are an electronic wave function and a vibrational wave function, respectively, and Q denotes a nuclear coordinate. $V_{nm}^{(1)}$ is a so-called direct spin−orbit interaction subject to the restrictive selection rule. $V_{nm}^{(2)}$ is a spin−orbit interaction induced by Herzberg−Teller vibronic coupling, and $V_{nm}^{(3)}$ is a spin−orbit interaction induced by Born−Oppenheimer vibronic coupling.[44,45]

We here considered ISC induced by the direct spin−orbit interaction between the 1^1B_1 and ^{3}MLCT states. In this case, the rate is expressed simply as the product of the square of the spin−orbit integral, $\langle{}^3\Phi_n(q,0)|H_{SO}(0)|{}^1\Phi_m(q,0)\rangle$, and FCWD (Franck−Condon-weighted density of the final vibronic states):

$$k(^1\mathrm{MLCT}_m \rightarrow {}^3\mathrm{MLCT}_n) = \frac{2\pi}{\hbar}|\langle{}^3\Phi_n(q,0)|H_{SO}(0)|{}^1\Phi_m(q,0)\rangle|^2\ \mathrm{FCWD} \quad (11)$$

where FCWD $= |\langle\chi_n|\chi_m\rangle|^2\ \rho(E_{^3\mathrm{MLCT}} = E_{^1\mathrm{MLCT}})$

The spin−orbit integrals between ^{3}MLCT and the lowest ^{1}MLCT (1^1B_1) were calculated using the procedure described in the Experimental Section and are shown in Figure 7a. Both

(44) Siebrand, W. *Chem. Phys. Lett.* **1970**, *6*, 192.
(45) Lawetz, V.; Orlandi, G.; Siebrand, W. *J. Chem. Phys.* **1972**, *56*, 4058.

ISC channels, $1^1B_1 \rightarrow 2^3A$ and $1^1B_1 \rightarrow 3^3B_2$, involve the spin−orbit integral of ca. 300 cm^{-1}. Such large values are ascribed to the large spin−orbit integrals between the metal-centered MOs (between HOMO and HOMO − 1 or between HOMO and HOMO − 2). However, both 2^3A and 3^3B_2 lie more than 5000 cm^{-1} higher than 1^1B_1 so that these ISC channels are strongly endothermic and thus possess very small FCWD. This is the case for the other lower-lying 2^1A, 1^1B_3, and 1^1B_2; all of the ISC channels with a large spin−orbit integral are strongly endothermic. Possible ISC due to spin−orbit interaction is therefore from 1^1B_1 to the lower-lying triplet states (1^3A, 1^3B_3, and 1^3B_2), and the corresponding spin−orbit integrals are less than 30 cm^{-1} working between ligand-centered MOs. Thus, this theoretical analysis definitely indicates that the large spin−orbit coupling of the 3d electron in these copper(I) compounds does not effectively work in the ISC from ^{1}MLCT to ^{3}MLCT, which is the reason that the copper(I) compounds exhibited prompt fluorescence with a relatively long lifetime.[46]

The sluggishness of the ISC is closely related to the flattening distortion of the ^{1}MLCT structure. Very fast ISC from singlet to triplet states in heavy metal compounds is ascribed to the spin−orbit integrals among MOs containing a large contribution of d atomic orbitals. Considering the FCWD of ISC processes, however, the energy of these MOs should not be very different. As for $[Cu(dmphen)_2]^+$, in pseudo D_{2d} geometry, $21b_2$ and $21b_3$ are almost energetically degenerated, and thereby, 2^3A (mixture of $21b_3 \rightarrow 22b_3$ and $21b_2 \rightarrow 22b_2$) lies near 1^1B_1 (mixture of $21b_2 \rightarrow 22b_3$ and $21b_3 \rightarrow 22b_2$). In this situation, both large spin−orbit integrals of ca. 300 cm^{-1} and an energetically preferable transition allow very fast ISC ($1^1B_1 \rightarrow 2^3A$); thus, the lifetime of the 1^1B_1 will be on the order of femtoseconds. However, when the dha decreases from 90°, $21b_2$ is destabilized and $21b_3$ is stabilized. Due to the changes in the MO energy, the state energy of 2^3A rises much higher than that of 1^1B_1 as shown in Figure 7a, and this ISC channel does not work.

As for $[Ru(bpy)_3]^{2+}$, HOMO($d\pi_{a1}$) lies 2.4 × 10^3 cm^{-1} above degenerate HOMO − 1 ($d\pi_{e-1}$ and $d\pi_{e-2}$).[47] Since these orbitals are nonbonding t_{2g} orbitals, the structural change in MLCT formation is quite small. The spin−orbit integral between $d\pi_{a1}$ and $d\pi_e$ is calculated to be ca. 300 cm^{-1} from Table 3 in ref 47, and $\zeta = 990$ cm^{-1}, and that between $d\pi_{e-1}$ and $d\pi_{e-2}$ is ca. 200 cm^{-1}. The former spin−orbit integral works slightly uphill (ca. 1000 cm^{-1}) ISC $^1A_2$-($d\pi_{a1} \rightarrow \pi^*a_2$) $\rightarrow$ $^3E(d\pi_e \rightarrow \pi^*a_2)$, and the latter induces downhill ISC $^1E(d\pi_e \rightarrow \pi^*a_2) \rightarrow {}^3E(d\pi_e \rightarrow \pi^*a_2)$, shortening the lifetime of ^{1}MLCT to the femtosecond time region. The integral of 300 cm^{-1} is 12 times larger than that (25.5 cm^{-1}) working in $[Cu(dmphen)_2]^+$, which indicates that the ISC rate in the ruthenium(II) compound is 150 times faster than that in the copper(I) compound according to eq 9 if the difference in FCWD is ignored. The difference in the spin−orbit integrals working in energetically favorable ISC channels account for a two-order difference in the lifetime of ^{1}MLCT between $[Ru(bpy)_3]^{2+}$ (40 ± 15 fs)[26] and the copper(I) compounds (ca. 15 ps) although the spin−orbit coupling constants of both the central metal ions are comparable.

Since the FC state retains the GS geometry (i.e., pseudotetrahedral), very fast ISC involving almost degenerate metal-centered MOs of $21b_2$ and $21b_3$ may be energetically favorable. Due to a large spin−orbit integral of the process (ca. 300 cm^{-1}), the ISC is likely to occur in the femtosecond time region at the GS geometry and competes with structural relaxation along with the potential energy surface of 1^1B_1 (process IC in Figure 8). The presence of such competition in the relaxation of the FC state is probably one reason for the small formation yield of the fluorescence state (ϕ = ca. 0.1) and its unusual dependence on the excitation wavelength. The small formation yield of the fluorescence state may be relevant to the parentage of the FC state. Since the oscillator strength of 2^1B_1 is much greater than that of 1^1B_1 at the GS geometry (Table 2), excitation with visible light mainly produces a vibronic state of 2^1B_1 as the FC state. The strong spin−orbit interaction between 2^1B_1 and 1^3A (Figure 7b) may induce very fast ISC superior to the relaxation to 1^1B_1. In copper(I) compounds having a flattened structure like the MLCT geometry, the formation of the fluorescence state may be efficient, and thereby, more intense prompt fluorescence will be observed.

Properties of the Phosphorescent State. Next, we discuss the origin and radiative rate of the phosphorescence (i.e., emission observed at the lower temperature of 173 K). The energy of the phosphorescence was 11.7 × 10^3 cm^{-1} (Figure 2), and the radiative rate constant estimated for phosphorescence was ca. 10^3 s^{-1}.[11] When band II was excited in highly viscous glycerin, the phosphorescence was found to be *z*-polarized, indicating that it originates from one component of the triplet state with B_1 symmetry.[18]

(46) ISC may be induced by higher order spin−orbit coupling ($V_{nm}^{(2)}$ or $V_{nm}^{(3)}$) involving state-mixing due to vibronic coupling with higher-lying virtual states. This mechanism is important especially when the direct spin−orbit interaction is symmetrically forbidden. Although evaluation of $V_{nm}^{(2)}$ or $V_{nm}^{(3)}$ is very difficult in a large molecule such as $[Cu(dmphen)_2]^+$, it is unlikely that the higher order interaction is superior to the direct interaction. To evaluate $V_{nm}^{(2)}$, weak dependence of the Φ on Q_k (Q_k is coordinate along the *k*-th normal mode) around the nuclear equilibrium configuration is assumed and is obtained from eq 10b:

$$V_{mm}^{(2)} = \sum_k [(\partial/\partial Q_k)\langle {}^3\Phi_n|H_{SO}|{}^1\Phi_m\rangle]_{Q_k=0}\langle\chi_n|Q_k|\chi_m\rangle = \sum_k \sum_i \left[\langle {}^3\Phi_n|H_{SO}|{}^1\Phi_i\rangle\left\langle {}^1\Phi_i\middle|\partial / \partial Q_k\middle|{}^1\Phi_m\right\rangle - \left\langle {}^3\Phi_n\middle|\partial / \partial Q_k\middle|{}^3\Phi_i\right\rangle \langle {}^3\Phi_i|H_{SO}|{}^1\Phi_m\rangle + \left\langle {}^3\Phi_n\middle|\partial H_{SO} / \partial Q_k\middle|{}^1\Phi_m\right\rangle\right]_{Q_k=0} \times \langle\chi_n|Q_k|\chi_m\rangle$$

The first term is the product of spin−orbit interaction in a triplet state ($^3\Phi_n$) with a higher-lying singlet virtual state ($^1\Phi_i$) and the degree of vibronic mixing of the virtual state with the initial singlet state ($^3\Phi_m$). The second term denotes the product of the degree of vibronic mixing in a triplet state ($^3\Phi_n$) with the higher-lying virtual triplet state ($^3\Phi_i$) and the spin−orbit interaction of that virtual state with the initial singlet state ($^1\Phi_i$). The third term $\langle {}^3\Phi_n|\partial H_{SO}/\partial Q_k|{}^1\Phi_m\rangle$ can be omitted due to its very small value. The most important higher order spin−orbit interaction must involve strong spin−orbit interaction between $1^1B_1 \leftrightarrow 2^3A$ (or 3^3B_2) (~300 cm^{-1}). However, the energy gap between these higher-lying triplet states (2^3A, 3^3B_2) and lower-lying triplet states (1^3A, 1^3B_1, 1^3B_3, 1^3B_2) is significant (> 4000 cm^{-1}) (Table 4). Therefore, the degree of state mixing between two groups of triplet states due to vibration, i.e., $\langle {}^3\Phi_n|\partial/\partial Q_k|{}^3\Phi_i\rangle$ term in the equation, is fairly small. Thus, the large value of $\langle {}^3\Phi_i|H_{SO}|{}^1\Phi_m\rangle$ seems to be canceled by the small value of $\langle {}^3\Phi_n|\partial/\partial Q_k|{}^3\Phi_i\rangle$ for all higher order spin−orbit interaction.

(47) Daul, C.; Baerends, E. J.; Vernooijs, P. *Inorg. Chem.* **1994**, *33*, 3538.

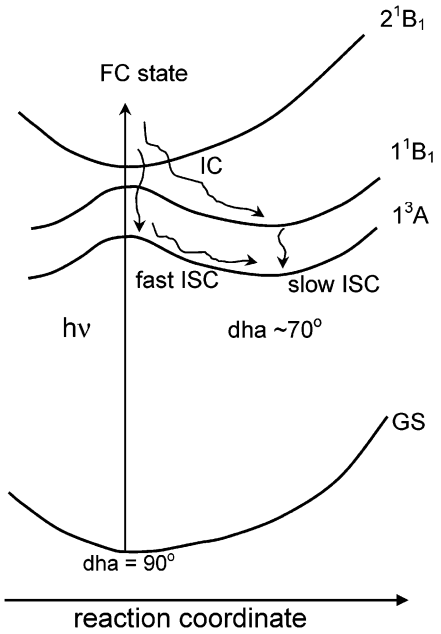

Figure 8. Probable relation pathway of FC state in photoexcited $[Cu(dmphen)_2]^+$ [FC = Franck−Condon, IC = internal conversion, ISC = intersystem crossing, dha = dihedral angle, GS = ground state, 1^1B_1 and 2^1B_1(^{1}MLCT), 1^3A(^{3}MLCT)].

When spin−orbit mixing occurs, the triplet state is perturbed by various singlet states. Three degenerated components in the lowest triplet state (1^3A) are split into three states (B_1, B_2, and B_3) by second-order spin−orbit interactions with singlet states. Under the Born−Oppenheimer approximation, the energy of these states is given by

$$E_{B_i} = E_{1^3A} + \sum_n \frac{H_{13}H_{31}}{E_{1^3A} - E_{n^1B_1}} |\langle \chi_{n^1B_1} | \chi_{1^3A} \rangle|^2 \quad (i = 1, 2, 3) \tag{12}$$

where $H_{13} = \langle \phi_{n^1B_i} | H_{SO} | \phi_{1^3A} \rangle$ and $H_{13} = \langle \phi_{1^3A} | H_{SO} | \phi_{n^1B_i} \rangle$. ϕ and E are eigenfunctions and eigenvalues of the Hamiltonian without spin−orbit coupling, respectively. The overlap integrals between the vibrational wave functions (χ) are assumed to be unity in the following calculations.

The lowest MLCT is B_1 although the energy splitting is very small (less than 10 cm^{-1}) (Scheme 2). The radiative rate constants of phosphorescence can be calculated from the transition dipole moments of singlet state components involved in the lowest triplet states as eq 13

$$k_r = \frac{16\pi^3 \times 10^6 \times \tilde{\nu}^3}{3h\epsilon_0} |M_{T \to GS}|^2 \tag{13}$$

where $\tilde{\nu}$ is the excitation energy of the triplet state at the wavenumber, and h and ϵ_0 are Planck's constant and the permittivity of vacuum, respectively. The transition dipole moment for phosphorescence $M_{T \to GS}$ is hence given by

$$M_{T \to GS} = \sum_n M_{n^1B_i \to GS} \times \frac{|H_{13}|}{(3E_{1^3A} - 1E_{n^1B_i})} |\langle \chi_{n^1B_i} | \chi_{1^3A} \rangle| \quad (i = 1, 2, 3) \tag{14}$$

Scheme 2. Comparison between the Observed and Calculated Properties of MLCT States of $[Cu(dmphen)_2]^+$ in CH_2Cl_2[a]

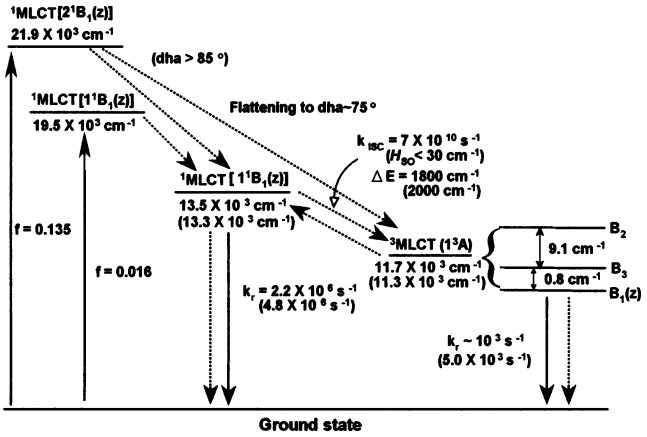

[a] Calcd values are in parentheses.

Table 5. Radiative Rate of Phosphorescence (k_r) as a Function of the dha in $[Cu(dmphen)_2]^+$[a]

dha/deg	k_r/s^{-1}
85	1.24×10^5
80	4.69×10^4
75	2.19×10^4
70	1.12×10^4
65	6.33×10^3
60	8.47×10^3

[a] The rates were calculated with the data in Table 2 using eqs 13, 14 and 15.

$$M = \sqrt{\frac{3he^2}{8\pi^2 m_e c\tilde{\nu}}} \cdot f \tag{15}$$

where m and e are the mass and charge of an electron, $\tilde{\nu}$ is the singlet-to-ground state transition energy in wavenumber, c is the speed of light, and f is the oscillator strength of the singlet state. The largest contribution of ^{1}MLCT in perturbed 1^3A is 2^1B_1 although the degree of perturbation is very small (contribution of 1.1×10^{-3}).

The k_r values calculated for B_1, B_2, and B_3 are 5.0×10^3, 1.2, and 28 s^{-1}, respectively. This calculation is in excellent agreement with that ($\sim 10^3$ s^{-1}) determined for ^{3}MLCT.[11] The largest contribution to the transition dipole moment comes from mixing with 2^1B_1. Hence, the phosphorescence borrows intensity from the $2^1B_1 \rightarrow$ GS transition. Although the spin−orbit interaction between 1^3A and 2^1B_1 is strong, a large difference in the energy (8.6×10^3 cm^{-1}) decreases the degree of mixing of these states.

The flattening distortion has a significant influence on the k_r values. As the dha decreases, the energy gap between 2^1B_1 and 1^3A increases, and the oscillator strength (f) between 2^1B_1 and GS decreases as shown in Table 2. Since the spin−orbit integral between these states is almost independent of the dha, the relationship in eq 14 indicates that the k_r value decreases with a decreasing dha. Table 5 shows the variation of k_r with the dha. The k_r value at 85° of the dha is about 10 times greater than that at 70°. Thus, the structural distortion (i.e., change in the dha) has a significant influence on k_r as well as on the ISC rate between ^{1}MLCT and ^{3}MLCT. The results in Table 5 favor the idea that copper(I) compounds

with long alkyl chains at 2,9-positions of phenanthrolines exhibit dramatic enhancement of the luminescence intensity in the frozen regime ($T \leq 120$ K).[11] This behavior was interpreted as a consequence of the blocking of the geometry to the ground state arrangement in the rigid matrix. The results shown in Table 5 rationalize that retaining the GS structure (i.e., dha = ca. 90°) enhances the phosphorescence intensity.

Conclusions

Prompt fluorescence from ^{1}MLCT of the copper(I) bis(diimine) compound was observed. The lifetime of ^{1}MLCT was ca. 15 ps. DFT studies revealed that the ISC channels induced by large spin−orbit interaction (ca. 300 cm^{-1}) between the metal-centered HOMO and HOMO − 1 were energetically unfavorable in the copper(I) compounds because the flattening distortion caused large splitting (6.9×10^3 cm^{-1}) between these orbitals, considerably decreasing the FCWDs of these channels. The possible ISC (^{1}MLCT → ^{3}MLCT) is therefore induced by small spin−orbit interactions (ca. 30 cm^{-1}) between the ligand-centered molecular orbitals.

Scheme 2 summarizes the photophysical properties of the MLCT states of $[Cu(dmphen)_2]^+$ in CH_2Cl_2 that illustrate the comparisons between the observed and the calculated values (in parentheses) based on the information obtained from DFT. Most of the calculated values are in excellent agreement with the observed ones, indicating that the current DFT calculation provides accurate information on the excited states even in compounds of heavy metal ions, giving valuable insights into their excited state properties.

Copper(I) bis(diimine) compounds with long alkyl chains at 2,9-positions of phenanthrolines are able to retard the excited state distortion and increase the luminescence intensity in the rigid matrix.[1] Our future work includes the photophysical investigations of these copper(I) compounds in various viscous solvents, which seem to be significant and relevant for further understanding of the dynamics of structural change on MLCT formation. The potential use of copper(I) compounds as sensitizers in regenerative solar cells has been explored extensively, especially from an economical and environmental viewpoint. If it is possible to increase the lifetime of ^{1}MLCT by regulating the ISC rates, it can widen the area of solar energy conversion processes acting as efficient electron transfer sensitizers in solar cells. Our experimental observations together with reliable DFT calculations may lead the understanding of the photophysics of copper(I) bis(diimine) compounds into a new and promising era.

In this study, the excited electron in the MLCT states of the copper(I) compounds was assumed to be delocalized over the ligands because it was calculated to be in the lowest state in the gas phase even without symmetry restriction. The time-resolved resonance Raman spectra for a solution of $[Cu(dmphen)_2]^+$, however, suggested that the excited electron is localized as $[Cu(II)(dmphen)(dmphen^-)]^+$.[48] Such a charged localization increases the solvent reorganization energy and thus increases the Stokes shift. Moreover, the localization is accompanied by symmetry lowering from D_2 to C_2. However, the weak spin−orbit interaction in the MLCT states of the copper(I) compounds is ascribed to the flattening structure owing to d^9 electronic configuration. Therefore, the localization of the excited electron would not cause substantial changes in the ISC mechanism although the strength of the interaction may vary to some extent. A theoretical study on a localized MLCT is under investigation.

Acknowledgment. Z.A.S. is grateful to the Japanese Ministry of Education, Science, Sports and Culture (Monbusho) for a graduate scholarship to pursue this research work. K.N. gratefully acknowledges financial support from Monbusho for a Grant-in-Aid for Scientific Research (12640556 and 13128206).

Supporting Information Available: Table of one-center one-electron spin−orbit matrix elements of $\langle \phi_A | ls | \phi_B \rangle$ in D_2 symmetry. This material is available free of charge via the Internet at http://pubs.acs.org.

IC034412V

(48) Gordon, K. C.; McGarvey, J. J. *Inorg. Chem.* **1991**, *30*, 2986.